HENRY GRANJON PRIZE COMPETITION 2012 Winner Category B: "Materials Behaviour and Weldability"

INFLUENCE OF THE [Cr_{eq}+Ni_{eq}] ALLOY LEVEL ON THE TRANSITION BETWEEN SOLIDIFICATION MODES IN AUSTENITIC STAINLESS STEEL WELD METAL

M. A. Valiente Bermejo

Dr. María Asunción VALIENTE BERMEJO (valiente.asun@gmail.com) is an independent consultant and researcher. (Barcelona, Spain).

ABSTRACT

It is well known that primary austenitic solidification modes [A, AF] are related to hot cracking susceptibility in the welding of austenitic stainless steels; therefore the transition between primary austenitic solidification mode [AF] and primary ferritic solidification mode [FA] is of utmost importance and traditionally has been related to a critical Cr_{eq}/Ni_{eq} ratio. This paper presents the experimental results obtained when analysing the effect of alloy level on the transition between solidification modes in austenitic stainless steel weld metals. With this aim, two series of compositions of austenitic stainless steel samples were prepared using an electric arc remelting furnace, keeping the overall alloying composition at two constant levels of [Cr_{eq}+Ni_{eq}] = 30 wt% and [Cr_{eq}+Ni_{eq}] = 40 wt% while changing the Cr_{eq}/Ni_{eq} ratio from 1.22 up to 2.00 in each series. The experimental results show that for an alloy level of [Cr_{eq}+Ni_{eq}] = 30 wt%, the critical Cr_{eq}/Ni_{eq} ratio for the [AF]/[FA] transition takes place between 1.38 and 1.55, while in case of [Cr_{eq}+Ni_{eq}] = 40 wt% the critical Cr_{eq}/Ni_{eq} ratio takes place between 1.28 and 1.32, which is lower in value and narrower in range than the values obtained for the lower alloyed series. A comparison between these experimental results and other authors' previous research is presented. Results reveal the importance of the alloy level [Cr_{eq}+Ni_{eq}] as a key parameter in the transition between solidification modes.

IIW-Thesaurus keywords: Arc welding; Austenitic stainless steels; Hot cracking; Solidification modes; Ferritic-Austenitic solidification mode; Austenitic-Ferritic solidification mode; Chromium equivalent; Nickel equivalent.

1 Introduction

Historically, the study of the hot cracking phenomenon during the stainless steel solidification in welding led researchers to discover the different solidification modes indirectly. Hot cracking can be experienced by austenitic stainless steels while being close to their melting point during welding, casting or hot forming, and the causes of the phenomenon have been extensively studied [1-17]. It has been demonstrated that during the primary solidification of austenite, impurities such as sulphur, phosphorus and boron tend to segregate to the liquid phase and form low melting point eutectics. The nature and distribution of these eutectics along the grain boundaries at the last stages of solidification together with the force of solidification shrinkage, the thermal contraction and the restraining forces are the main causes of hot cracking. It has also been demonstrated that if the material solidifies as primary δ-ferrite, then it will experience the solid state transformation δ→γ. As the result, the material will be less susceptible to hot cracking due to the higher solubility of impurities in the δ phase as well as the better cracking resistance of δ/γ interfaces than δ/ δ or γ/γ interfaces where the eutectic liquid enriched with impurities has better grain boundary wettability.

Despite that the phenomenon has been known for a long time, it was not until 1979 that Suutala *et al.* [2] published their first research work relating the hot cracking of stainless steel welds to the solidification mode. They found that there was a critical value for the ratio of Chromium equivalent (Cr_{eq}) and Nickel equivalent (Ni_{eq}), $Creq/Ni_{eq}$ (Cr_{eq}/Ni_{eq} = 1.48 Schaeffler equivalents [18]), which established

Doc. IIW-2290 recommended for publication by Commission IX "Behaviour of Metals Subjected to Welding".

the boundary between the primary austenitic solidification mode and the primary ferritic solidification mode and that this critical value also outlined the boundary for hot cracking susceptibility of stainless steel welds.

During the course of research up to 1983, Suutala ***et al.*** [3, 6-8] progressed in the field with the establishment of four solidification modes: austenitic [A], austenitic-ferritic [AF], ferritic-austenitic [FA] and ferritic [F]. Suutala ***et al.*** also stated that the Hammar and Svensson (H&S) equivalents [19] gave a better correlation between composition and solidification modes than Schaeffler [18] and DeLong [20] equivalents, and they established the critical value for the transition between primary austenitic and primary ferritic solidification modes at $Cr_{eq}/Ni_{eq} = 1.50$ (H&S).

From the Suutala ***et al.*** research, the solidification modes have been an independent and consolidated matter to study, and later on, authors such as Elmer ***et al.*** [21] and Inoue ***et al.*** [22-24] studied the mechanisms of solidification modes in depth and their relationship with the morphologies and crystallographic orientations of the residual δ-ferrite.

According to references [10, 21, 25-28], the main factor that influences the solidification mode is the chemical composition (expressed as Cr_{eq}/Ni_{eq}). However, in those alloys for which chemical composition is close to the eutectic-peritectic reaction, and consequently falls in the three-phase (L+δ+γ) zone of the ternary Fe-Cr-Ni phase diagram, the cooling rate is the key parameter to determine if the solidification mode will be [AF] or [FA].

In recent years, large numbers of studies have been carried out to investigate the effect of high cooling rate processes (10^4-10^7 °C/s) like Laser Beam Welding (LBW) and Electron Beam Welding (EBW) on the austenitic stainless steels solidification mode [8, 10, 12, 21, 26, 29-31]. It has been demonstrated that higher cooling rate promotes austenite as the primary solidification phase due to the dendrite tip undercooling phenomenon [10, 12, 26, 30, 32-34] and consequently samples which solidify in the form of [FA] under arc welding conditions can become [A] under the cooling conditions of EBW. Some authors have proposed critical levels of Cr_{eq}/Ni_{eq} ratio for the transition [AF]/[FA]. For example, Brooks [10, 12, 13] and Lippold [26] reported that the transition under laser conditions occurred at a Cr_{eq}/Ni_{eq} ratio around 1.65 (using WRC-1992 equivalents [35]) and 1.7 (using Schaeffler equivalents [18]).

Differing from previous research, this paper takes into consideration the effect of overall alloy level [Cr_{eq}+Ni_{eq}] on the transition between [AF] and [FA] solidification modes in austenitic stainless steel weld metals.

2 Experimental procedure

Two series of samples were designed and prepared, one consisted of 17 samples with a constant total alloying level of [Cr_{eq}+Ni_{eq}]= 40 wt% and the second one consisted of 15 samples with a constant alloying level of [Cr_{eq}+Ni_{eq}] = 30 wt%. Whereas the alloying level is kept constant, the Cr_{eq}/Ni_{eq} ratio has been gradually increased from 1.22 up to 2.00 in steps between 0.10 and 0.70. Chromium and Nickel equivalents are calculated using the equations established by Hammar and Svensson [19] (Equations 1.a,b).

In a previous research by the author [36] related to the development of a mathematical model for Ferrite Number (FN) prediction, it was found that the use of Hammar and Svensson equivalents resulted in lower error for FN predictions than using WRC-1992 equivalents [35]. Also it was considered that Suutala ***et al*** [3, 6-8], who established the solidification modes, stated that Hammar and Svensson equivalents gave a better correlation between composition and solidification modes than Schaeffler's or DeLong's ones.

$$Cr_{eq} = Cr + 1.37\ Mo \quad (1.a)$$

$$Ni_{eq} = Ni + 0.31\ Mn + 22\ C + 14.2\ N \quad (1.b)$$

The feed materials used for sample preparation are three grades of solid wires for Gas Tungsten Arc Welding (GTAW), one mild steel grade and two austenitic stainless steel grades, so that intended different alloying compositions were prepared using different weight combinations of these wires. Table 1 shows the designations and chemical compositions of these wires.

The wires were cleaned, cut in segments between 10-18 mm length, weighted and mixed in different proportions so that the designed different levels of [Cr_{eq}+Ni_{eq}] and Cr_{eq}/Ni_{eq} ratios were achieved, as shown in Tables 2 and 3. The total weight of each batch of the samples was 50 g which were melted in a pure argon atmosphere using the electric arc remelt furnace depicted in

Table 1 – Chemical composition of the base materials used (wt%)

AWS Designation	Lot	C	Mn	Si	S	P	Cr	Ni	O	N
ER310	WO11557	0.108	1.70	0.34	0.0018	0.013	25.92	20.65	0.008	0.043
ER70S-6	WO20929	0.076	1.43	0.81	0.0112	0.011	0.025	0.015	0.010	0.003
ER312	WO14634	0.105	1.85	0.41	0.0006	0.021	30.31	9.15	0.010	0.151
ER312	WO11381	0.105	1.80	0.31	0.0005	0.023	30.35	9.12	0.010	0.087

Table 2 – List of samples series [Cr_{eq}+Ni_{eq}] = 40 wt%, prepared from weight combination of three grades of solid wires (ER310, ER312 and ER70S-6)

Cr_{eq}/Ni_{eq}	Cr_{eq}+Ni_{eq} wt%	ER310		ER312			ER70S-6		Sample weight g
		wt%	g	wt%	g		wt%	g	
1.22	40.49	61.97	30.99	20.20	10.10	(a)	17.83	8.92	50.01
1.28	40.58	57.01	28.50	26.01	13.00	(a)	16.98	8.49	49.99
1.32	40.58	52.59	26.29	30.99	15.49	(a)	16.42	8.21	49.99
1.38	40.61	47.70	23.85	36.60	18.30	(a)	15.70	7.85	50.00
1.43	40.68	43.50	21.75	41.50	20.75	(a)	15.00	7.50	50.00
1.44	40.66	42.50	21.25	42.60	21.30	(a)	14.90	7.45	50.00
1.46	40.67	41.10	20.56	44.18	22.10	(a)	14.72	7.36	50.02
1.48	40.71	39.50	19.74	46.10	23.04	(a)	14.40	7.20	49.98
1.54	40.00	38.00	19.00	47.00	23.50	(b)	15.00	7.50	50.00
1.59	40.02	35.00	17.50	50.50	25.25	(b)	14.50	7.25	50.00
1.64	40.81	28.20	14.10	59.10	29.55	(a)	12.70	6.35	50.00
1.68	40.81	25.03	12.51	62.69	31.34	(a)	12.28	6.14	49.99
1.73	40.02	26.40	13.20	60.40	30.20	(b)	13.20	6.60	50.00
1.78	40.00	23.50	11.75	63.70	31.85	(b)	12.80	6.40	50.00
1.83	40.01	21.00	10.50	66.60	33.30	(b)	12.40	6.20	50.00
1.89	40.02	17.90	8.95	70.20	35.10	(b)	11.90	5.95	50.00
2.00	40.02	12.00	6.00	77.00	38.50	(b)	11.00	5.50	50.00

(a) lot WO14634 and (b) lot WO11381. Different lots of ER312 wire.

Table 3 – List of samples series [Cr_{eq}+Ni_{eq}] = 30 wt%, prepared from weight combination of three grades of solid wires (ER310, ER312 and ER70S-6)

Cr_{eq}/Ni_{eq}	Cr_{eq}+Ni_{eq} wt%	310S94		312S94			ER70S-6		Sample weight g
		wt%	g	wt%	g		wt%	g	
1.22	30.34	41.71	20.86	19.18	9.59	(a)	39.11	19.56	50.01
1.28	30.37	37.49	18.74	24.00	12.00	(a)	38.51	19.25	49.99
1.33	30.40	34.29	17.14	27.70	13.85	(a)	38.01	19.00	49.99
1.38	30.40	31.19	15.60	31.19	15.60	(a)	37.62	18.81	50.01
1.43	30.44	27.92	13.96	34.98	17.49	(a)	37.10	18.55	50.00
1.48	30.49	25.02	12.51	38.39	19.19	(a)	36.59	18.29	49.99
1.55	30.00	24.00	12.00	39.10	19.55	(b)	36.90	18.45	50.00
1.61	30.23	21.20	10.60	42.90	21.45	(b)	35.90	17.95	50.00
1.68	30.25	18.19	9.10	46.40	23.21	(b)	35.41	17.71	50.02
1.73	30.01	15.70	7.85	48.70	24.35	(b)	35.60	17.80	50.00
1.79	30.01	13.00	6.50	51.80	25.90	(b)	35.20	17.60	50.00
1.85	30.25	10.90	5.45	54.80	27.40	(b)	34.30	17.15	50.00
1.90	30.28	8.70	4.35	57.40	28.70	(b)	33.90	16.95	50.00
1.96	30.26	6.40	3.20	60.00	30.00	(b)	33.60	16.80	50.00
2.00	30.00	5.00	2.50	61.00	30.50	(b)	34.00	17.00	50.00

(a) lot WO14634 and (b) lot WO11381. Different lots of ER312 wire.

Figure 1, based on the GTAW process which is recommended by the ASTM E1306-94 standard [37]. In previous detailed research on this standard by the current author [38], evidences of compositional heterogeneity were found and some modifications were recommended to the ASTM procedure in order to ensure homogeneous samples. Consequently, ASTM issued a new revision to the standard, ASTM E1306-07 [39]. The same work [38] demonstrated that, for a satisfactory sample, the optimum parameters for the remelting process were; current 550 A, voltage 30 V, holding duration 60 s followed by 3 minutes cooling inside the furnace. Accordingly, these settings were applied to all sample preparation of the current work. In the same previous research, it was determined by DAS (Dendrite Arm Spacing) that the samples prepared using this electric arc furnace were cooled at 10 °C/s.

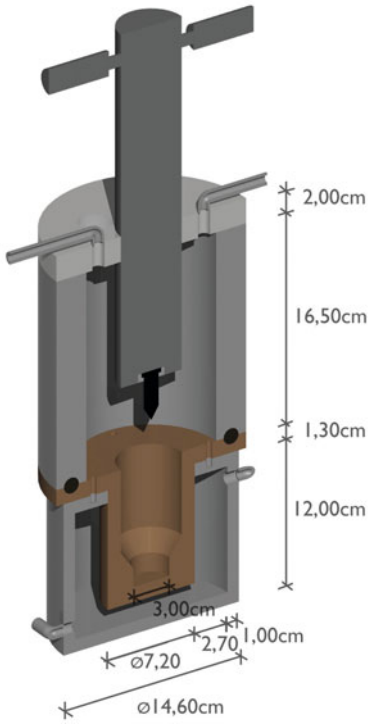

Figure 1 – Schematic illustration of the electric arc remelting furnace used for samples preparation

Figure 2 – Picture of the upper and lower half-button surfaces once the sample has been cut in order to start the metallographic preparation procedure of its transverse cross-section

This cooling rate is on the low side for most arc welding processes, but is in agreement with possible cooling rates experienced by these processes, whose orders of magnitude can be found between 10-10^3 °C/s [8, 19, 32].

The solid and homogeneous samples obtained were cut into two halves (Figure 2) by a cooled sawblade and the transverse cross-section (Figure 3) was ground and polished according to standard metallographic preparation procedures. The etchants used were Kalling's n° 2 reagent and ferrofluid EMG 911. These etchants demonstrated the best resolution out of the 8 different etchants tested in the previous study [38].

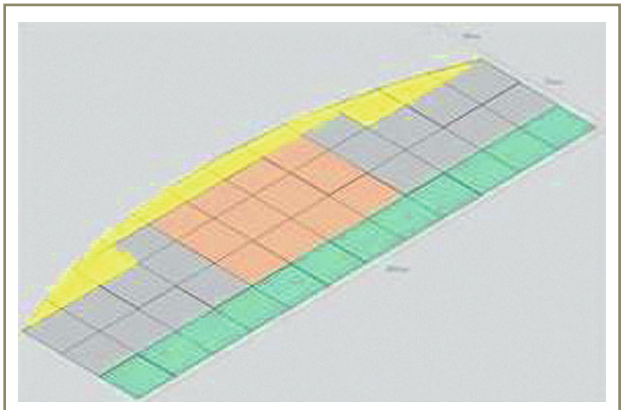

Figure 3 – Transverse cross-section zones defined: upper (yellow) in contact with the inert gas, central (rose) and lower (green) in contact with the copper crucible

Optical Microscopy (Axiovert 100A + Delta Pix Viewer LE Software) and Scanning Electron Microscopy (SEM) equipped with Energy Dispersive X-ray Spectroscopy (EDS) (LEICA-Stereoscan 360) were used for microstructural characterisation. Occasionally, for higher resolution, Field Emission (FEG-SEM) equipment (Hitachi S-4100) was also used.

As depicted in Figure 3, three different areas could be defined on the overall transverse surface: the upper one (coloured in yellow) which was in contact with the inert gas, the lower one (coloured in green) which was in contact with the copper crucible and the central one (coloured in rose). The central zone was specifically investigated. Two main reasons supported this selection; first, this zone was more convenient for metallographic inspection and DAS determination of cooling rate, and second, as the initial research also involved FN measurements by Feritscope [36], the selection of the central area avoided the edge effect phenomenon associated to a drop in the measured FN values when taking measurements near the edge of the sample.

3 Experimental results and discussion

Results are presented in the following order: first, a characterisation of each solidification mode is depicted, including the values of Cr_{eq}/Ni_{eq} ratio which show each solidification mode at each alloy series. Table 4 summarises the above mentioned results obtained from the microstructural analysis of the central zone of the sample's transverse cross-section. Second, the transition between [AF] and [FA] is discussed and the effect of the cooling rate is also considered. Finally, a comparison between the experimental results and some previous research is made.

3.1 Austenitic solidification mode [A]

In the [Cr_{eq}+Ni_{eq}]= 40 wt% series, the sample with the lowest Cr_{eq}/Ni_{eq} ratio (1.22) shows an [AF] solidification

Table 4 – Summary of experimental results. Solidification modes vs. Cr_{eq}/Ni_{eq} and [Cr_{eq}+Ni_{eq}]

Series [Cr_{eq}+Ni_{eq}] = 40 wt%			Series [Cr_{eq}+Ni_{eq}] = 30 wt%		
Ref.	Cr_{eq}/Ni_{eq}	Mode	Ref.	Creq/Ni_{eq}	Mode
A18	1.22	AF	A36	1.22	A
A21	1.28	AF/FA	A39	1.28	A
A24	1.32	AF/FA	A42	1.33	AF
A27	1.38	FA	A45	1.38	AF/FA
A30	1.43	FA	A48	1.43	AF/FA
A31	1.44	FA	A51	1.48	AF/FA
A32	1.46	FA	A531	1.55	AF/FA
A33	1.48	FA	A74	1.61	FA
A54R	1.54	FA	A77	1.68	FA
A57R	1.59	FA	A80R	1.73	FA
A60	1.64	FA	A83R	1.79	FA
A63	1.68	FA	A86	1.85	FA
A66R	1.73	FA	A89	1.90	FA
A69R	1.78	F	A92	1.96	FA
A711	1.83	F	A94	2.00	FA/F
A714	1.89	F			
A731	2.00	F			

mode, therefore this series does not show any pure austenitic solidification mode [A]. However, the [A] solidification mode is clearly observed in the [Cr_{eq}+Ni_{eq}] = 30 wt% series among the samples with the Cr_{eq}/Ni_{eq} ratio ranging between 1.22 and 1.28. This indicates that, for a composition of lower alloy level, a higher Cr_{eq}/Ni_{eq} ratio is required for the transition between [A] and [AF] solidification modes to occur.

Figure 4 illustrates the [A] solidification mode shown in sample A39 (Cr_{eq}/ Ni_{eq}= 1.28, [Cr_{eq}+Ni_{eq}] = 30 wt%), which presents only an austenite phase in dendritic morphology throughout the transverse cross-section analysed. Despite no δ-ferrite observed in the interdendritic boundary, the local microanalysis of sample A39 shown in Figure 5 demonstrates the fact that Cr experienced compositional segregation during solidification, with the interdendritic boundary enriched and the dendrite core depleted in Cr.

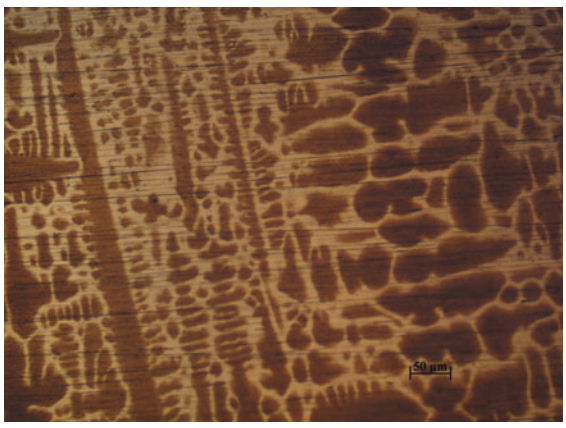

Figure 4 – [A] solidification mode in sample A39 (Cr_{eq}/Ni_{eq} = 1.28, [Cr_{eq}+ Ni_{eq}] = 30 wt%)

3.2 Austenitic-Ferritic solidification mode [AF]

A pure Austenitic-Ferritic solidification mode was observed at Cr_{eq}/Ni_{eq} = 1.22 in the [Cr_{eq}+Ni_{eq}] = 40 wt% series, and at Cr_{eq}/Ni_{eq} = 1.33 in the [Cr_{eq}+Ni_{eq}] = 30 wt% series. Figure 6 illustrates the above mentioned solidification mode shown by sample A18 (Cr_{eq}/Ni_{eq} = 1.22, [Cr_{eq}+Ni_{eq}] = 40 wt%). It presents dendrites of γ-austenite in the majority and some vermicular/globular δ-ferrite in the minority, which is always located at the interdendritic boundary. Additionally, Figure 7 depicts the results obtained from a linear EDS microanalysis traversing an austenite/interdendritic δ-ferrite/austenite line also in sample A18, where the chromium enrichment and the nickel depletion in the δ-ferrite phase are evident.

These experimental observations are in agreement with the solidification mechanism proposed by previous researchers [1, 10, 15, 22, 31] whereby the austenite phase starts its solidification first and δ-ferrite solidifies from the last interdendritic liquid which has been enriched in Cr due to compositional segregation during the earlier stage of the solidification process. It is also agreed that the mechanism of δ-ferrite formation is related to the eutectic reaction L→γ+δ. The residual ferrite is a divorced eutectic and it is known by different designations depending on the authors: eutectic ferrite [5, 10, 12, 14, 26, 31, 40-43], interdendritic ferrite [15, 21, 31, 44], vermicular ferrite [2] or globular ferrite [22].

3.3 Ferritic-Austenitic solidification mode [FA]

A pure Ferritic-Austenitic solidification mode was observed at Cr_{eq}/Ni_{eq} = (1.38-1.73) in the [Cr_{eq}+Ni_{eq}] = 40 wt%

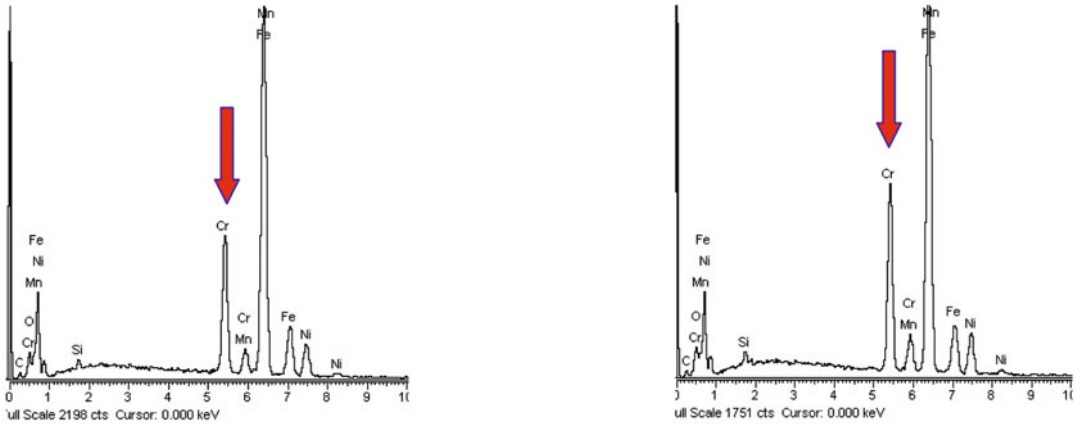

a) dendrite core

b) dendrite boundary

Figure 5 – EDS microanalysis in sample A39 (Cr_{eq}/Ni_{eq} = 1.28, [Cr_{eq}+Ni_{eq}] = 30 wt%) showing compositional segregation of chromium during solidification

series, and at Cr_{eq}/Ni_{eq} = (1.61-1.96) in the [Cr_{eq}+Ni_{eq}] = 30 wt% series. It is noticeable that a higher level of alloy favours the presence of ferrite at lower Cr_{eq}/Ni_{eq} ratios. Two different δ-ferrite morphologies were observed during the microstructural characterisation of the samples; skeletal ferrite (Figure 8) and lathy/lacy ferrite (Figure 9). It was observed that the skeletal morphology was present at low Cr_{eq}/Ni_{eq} ratios in the range of the [FA], while the lathy morphology was observed at higher Cr_{eq}/Ni_{eq} ratios within the range.

The mechanism responsible for the [FA] solidification mode has been widely agreed among researchers [10, 14, 15, 22, 40-42, 45], and it is briefly summarised below. Those alloys whose composition falls into the three-phase area (L+δ+γ) of the Fe-Cr-Ni phase diagram start their solidification with δ-ferrite phase, but before the end of the solidification, some γ-austenite is formed in equilibrium with the δ-ferrite and the last liquid. It is known as peritectic-eutectic reaction, however, the ternary composition which establishes the transition point between the peritectic reaction (L+δ→γ) and the eutectic reaction (L→δ+γ) under welding conditions is not clear yet. The complete phase transformation reactions in this solidification mode are L→L+δ→L+δ+$(δ+γ)_{per-eut}$→δ+γ.

The compositional segregation taking place at the solid/liquid interface during solidification was also studied by

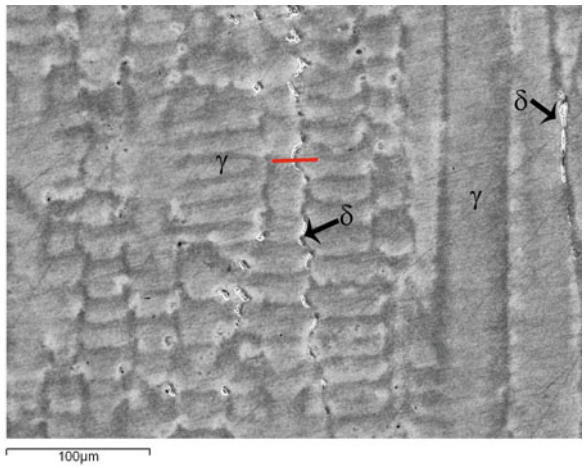

Figure 6 – [AF] solidification mode in sample A18 (Cr_{eq}/Ni_{eq} = 1.22, [Cr_{eq}+Ni_{eq}] = 40 wt%) showing dendrites of austenite in the majority and some eutectic ferrite at the interdendritic boundaries. The red line represents the location of the linear EDS microanalysis presented in Figure 7

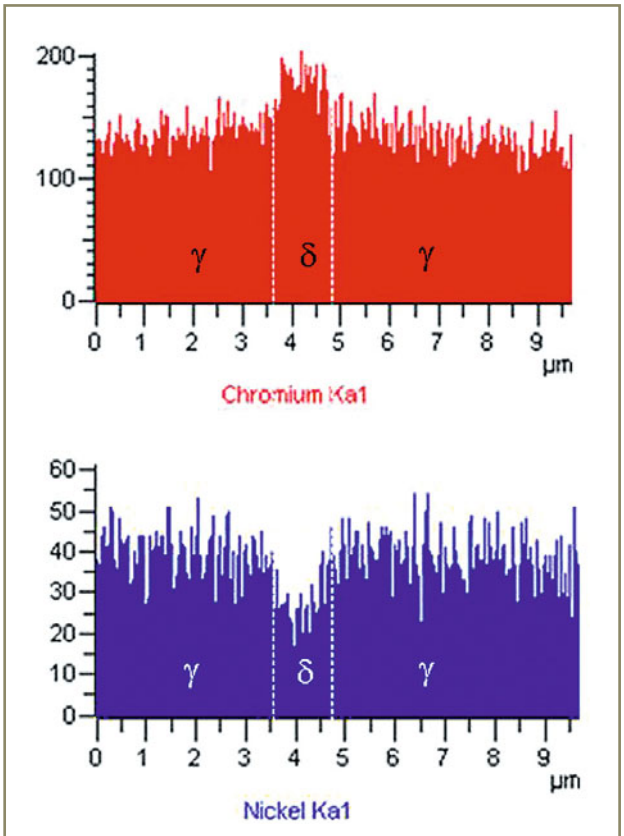

Figure 7 – Linear EDS microanalysis on dendrite boundary in sample A18 (Cr_{eq} / Ni_{eq} = 1.22, [Cr_{eq}+ Ni_{eq}] = 40 wt%) showing chromium enrichment and nickel depletion in the δ-ferrite phase

researchers [14, 22, 41, 43, 44, 46] and it was concluded that this is responsible for the δ-ferrite enrichment in Cr and depletion in Ni, and as a consequence the interdendritic liquid enrichment in Ni enhances the above mentioned austenite formation in the last stage of solidification. At the same time, the Cr enrichment of the primary δ-ferrite dendrite cores prevents the transformation δ→γ which takes place during cooling, and the skeletal morphology depicted at room temperature is the result of the unaffected δ-ferrite cores.

The solid state transformation δ→γ from primary δ-ferrite being transformed into secondary γ-austenite is controlled by diffusion; therefore the cooling rate influences the progress of the transformation. Higher cooling rates will lead to a lower degree of diffusion and hence less γ-austenite formation; therefore higher residual δ-ferrite content will be expected.

Regarding the different δ-ferrite morphologies observed, they can be explained according to Inoue *et al.* [22-24]. When the δ-ferrite and the primary austenite grow parallel to the heat flow direction, but without specific crystallographic orientation at the δ/γ interface during solidification, the secondary austenite grows planar towards the centre of the ferrite dendrite, keeping interface incoherence and resulting in a skeletal ferrite morphology. On the contrary, samples which have the Kurdjumov-Sachs crystallographic orientation between δ-ferrite and primary austenite during solidification will keep the same crystallographic orientation at the δ/γ interface during the solid state transformation, and the secondary austenite grows epitaxially from the grain boundary to the centre of the primary δ-ferrite dendrite, thus forming the lathy morphology. It is known that the lathy morphology increases the efficiency of the diffusion during the solid state transformation δ→γ when diffusion is restricted.

3.4 Ferritic solidification mode [F]

The composition of the [Cr_{eq}+Ni_{eq}] = 40 wt% series presents the Ferritic solidification mode when Cr_{eq}/Ni_{eq} reaches 1.78 and above, while the [Cr_{eq}+Ni_{eq}] = 30 wt% series only presents this solidification mode at Cr_{eq}/Ni_{eq} = 2.00 in coexistence with the [FA]. The microstructure observed for a Cr_{eq}/Ni_{eq} ratio between 1.78-1.89 was acicular ferrite in an austenitic matrix as shown in Figure 10. Only when Cr_{eq}/Ni_{eq} = 2.00 in the 40 wt% series it was possible to observe the Widmanstätten austenite plates, as Figure 11 depicts.

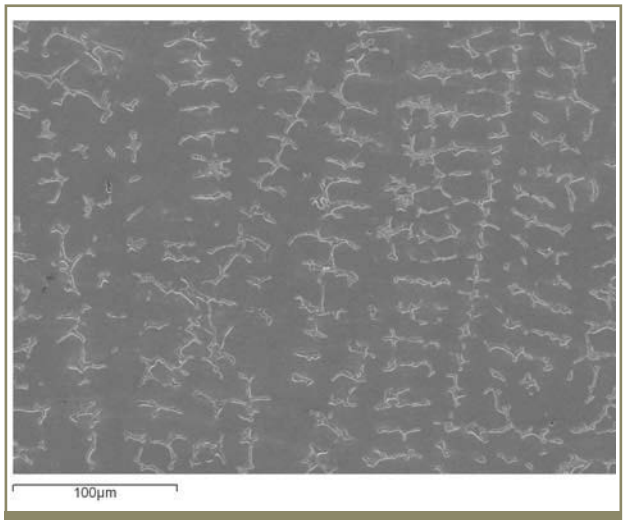

Figure 8 – Skeletal ferrite morphology in [FA] Sample A33 (Cr_{eq}/Ni_{eq} = 1.48, [Cr_{eq}+Ni_{eq}] = 40 wt%)

Figure 9 – Lathy ferrite morphology in [FA] Sample A32 (Cr_{eq}/Ni_{eq} = 1.46, [Cr_{eq}+Ni_{eq}] = 40 wt%)

According to references [22, 40, 46] the mechanism related to the [F] solidification mode follows the global reaction L→L+δ→δ→δ+γ. When solidification finishes, only dendrites of δ-ferrite are present. During further cooling this primary ferrite transforms into secondary austenite, and such solid state transformation δ→γ will be controlled by diffusion and consequently the cooling rate will limit the degree of the transformation. Researchers have also found that for moderate cooling rates and low Cr_{eq}/Ni_{eq} ratios in the [F] range, the transformation takes place with an acicular ferrite morphology, while for higher Cr_{eq}/Ni_{eq} ratios, the transformation takes place at lower temperatures and the microstructure observed is a ferritic matrix with Widmanstätten austenite plates. Inoue *et al.* [22] found that, independent of the austenite morphology formed in the solid state transformation, the crystallographic orientation between the primary δ-ferrite and the γ-austenite followed the Kurdjumov-Sachs relationship.

3.5 Transition between [AF] and [FA] solidification modes

During the course of the current research, the simultaneous coexistence of [AF] and [FA] solidification modes in a range of samples has been observed. For the [Cr_{eq}+Ni_{eq}] = 40 wt% series, the coexistence takes place in samples within the range Cr_{eq}/Ni_{eq} = (1.28-1.32) while for the [Cr_{eq}+Ni_{eq}] = 30 wt% series the coexistence is observed within the range Cr_{eq}/Ni_{eq} = (1.38-1.55). The lower alloyed series experiences the transition at higher Cr_{eq}/Ni_{eq} values and the coexistence is observed in a wider interval. Therefore, these experimental results show that the transition between [AF]/[FA] solidification modes depends on

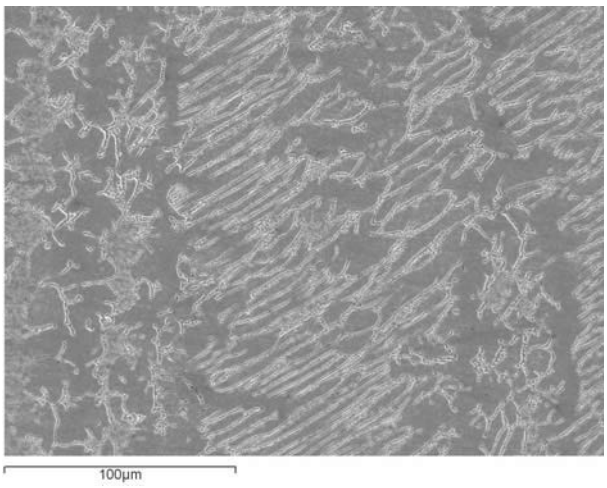

a) Sample A69R (Cr_{eq}/Ni_{eq} = 1.78, [Cr_{eq}+Ni_{eq}] = 40 wt%)

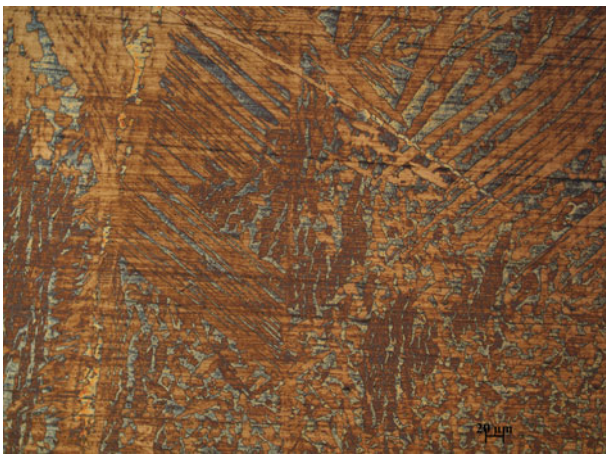

b) Sample A94 (Cr_{eq}/Ni_{eq} =2.00, [Cr_{eq}+Ni_{eq}] = 30 wt%)

Figure 10 – Acicular ferrite morphology in [F] solidification mode.

Figure 11 – Widmanstätten austenite in [F] solidification mode. Sample A731 (Cr_{eq}/Ni_{eq} = 2.00, [Cr_{eq}+Ni_{eq}] = 40 wt%)

the alloy level and that the lower alloyed alloys need a higher Cr_{eq}/Ni_{eq} ratio to experience the transition.

Figure 12 a) and b) illustrate the coexistence of primary austenite dendrites and eutectic ferrite at the interdendritic boundary which is indicative of [AF], with skeletal ferrite which confirms also primary ferritic dendrites and indicates the [FA] solidification mode. From the observation of the group of samples showing [AF] and [FA] coexistence, three aspects have been observed when Cr_{eq}/Ni_{eq} is increased. First, coexistence is observed at the lower and central zones of the transverse cross-section (Figure 3), while the upper zone only presents the [AF] solidification mode. Second, as the ratio increases, [FA] is found in greater proportion than [AF] and it was also found that in the ferrite morphologies related to [FA], they started with a skeletal morphology for low Cr_{eq}/Ni_{eq} ratios and followed with a coexistence between skeletal and

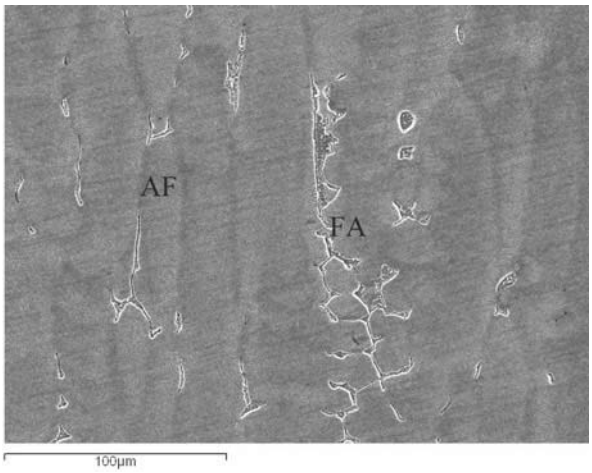

a) Sample A21 (Cr_{eq}/Ni_{eq} = 1.28 [Cr_{eq}+Ni_{eq}] = 40wt%) transverse lower section

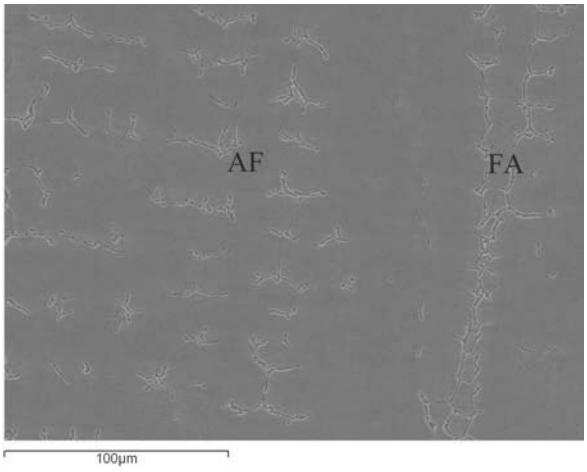

b) Sample A24 (Cr_{eq}/Ni_{eq} = 1.32 [Cr_{eq}+Ni_{eq}] = 40wt%) transverse central section

Figure 12 – Coexistence of eutectic ferrite [AF] and skeletal ferrite [FA]

lathy morphologies for higher ratios. Third, as depicted in Figure 13, the effect of the solid state transformation $\delta \rightarrow \gamma$ becomes more evident for both ferrite morphologies with rising Cr_{eq}/Ni_{eq}, and it is possible to observe the effect of the secondary austenite progressing towards the centre of the primary ferrite.

As stated above, the distribution of solidification modes on the transverse cross-section shows [AF] in the upper zone and coexistence of [AF] and [FA] in the central and lower regions. This distribution could be explained by two phenomena: the compositional segregation taking place at the solid/liquid interface during solidification, and the presence of a gradient in cooling rates within the sample could enhance a shift in the solidification modes, especially in those samples whose compositions allow the coexistence of three-phase (L+δ+γ) during solidification.

It is not possible to establish a quantified correlation between the local distribution of solidification modes on the transverse cross-section and the local level of δ-ferrite (measured as Ferrite Number, FN). However, it is possible to have the average FN value per each zone of the transverse cross-section. Sixty individual measurements were taken per zone in a previous research by the current author [36, 38], and their average values are shown in Table 5. The standard deviations of the average values are in the range between +/- 0.4 up to +/- 3.0, which are lower than the Feritscope tolerances for the specific FN band.

Measurements were taken by using a properly calibrated Feritscope, which is based on magnetic permeability fundamentals and it has an inherent limitation associated to the measurements taken at distances lower than 5 mm to the edge of the sample. This edge effect is a source of error in the measurements taken in the upper and lower zones of the transverse cross-section, therefore, their corresponding values shown in Table 5 cannot be considered as absolute values. However, as the error is supposed to be of the same extent in both zones, it is possible to compare the general behaviour of the data and correlate them with the local distribution of the solidification modes. Therefore, it is possible to conclude that the upper zone which only shows [AF] solidification mode has lower FN values than the central and lower zones of the transverse cross-section which have [FA] and [AF] coexistence.

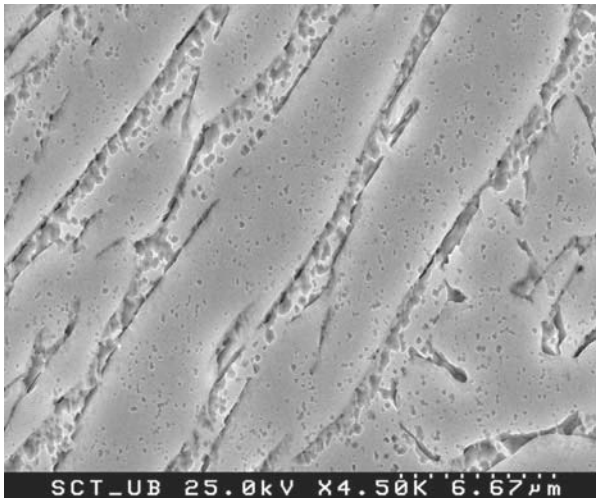

Figure 13 – Effect of $\delta \rightarrow \gamma$ on lathy ferrite. Sample A714 (Cr_{eq}/Ni_{eq} = 1.89 [Cr_{eq}+Ni_{eq}] = 40 wt%)

3.6 Comparison between experimental results and previous research

Since 1979 until today, different research have been carried out to establish the critical Cr_{eq}/Ni_{eq} ratio related to the transition between [AF]/[FA] solidification modes under arc welding conditions. Table 6 summarises the results and conditions of those previous works. The experimental results from the current research and also the predicted

Table 5 – Average FN values in the transverse cross-section zones of samples with [AF]/[FA] coexistence [36, 38]

Ref.	Cr_{eq}+Ni_{eq}	Cr_{eq}/Ni_{eq}	FN average Upper zone	FN average Central zone	FN average Lower zone
A21	40 wt%	1.28	1.1	0.8	0.7
A22R	40 wt%	1.30	1.8	1.7	1.4
A23	40 wt%	1.31	1.7	2.3	2.0
A24	40 wt%	1.32	2.2	3.1	3.1
A45	30 wt%	1.38	0.2	0.5	0.5
A46R	30 wt%	1.40	0.6	1.0	0.7
A47	30 wt%	1.41	0.3	0.6	0.8
A48	30 wt%	1.43	0.5	0.9	1.0
A49	30 wt%	1.45	0.6	0.9	1.2
A50	30 wt%	1.47	0.7	1.2	1.1
A51	30 wt%	1.48	0.6	0.9	1.4
A52R	30 wt%	1.50	1.8	2.6	2.9
A53	30 wt%	1.53	1.2	2.1	3.2
A531	30 wt%	1.55	2.1	4.4	3.5

Table 6 – Comparison between experimental results and previous research in [AF]/[FA] transitions

Researcher	Process	Cooling rate	Equivalents	Critical Cr_{eq}/Ni_{eq}	Alloy level (Cr_{eq}+ Ni_{eq})
Suutala *et al.* [2, 3]	SMAW and GTAW	N.S.	Schaeffler [18] Cr_{eq} = Cr + Mo + 1.5Si + 0.5Nb Ni_{eq} = Ni + 0.5Mn + 30C	1.48 $(1.58)_{H\&S}$	39 wt% $(39\ wt\%)_{H\&S}$
Hammar & Svensson [19]	Induction furnace	0.33 °C/s	Hammar & Svensson Cr_{eq} = Cr + 1.37Mo Ni_{eq} = Ni + 0.31Mn + 22C + 14.2N	1.35	Regression analysis range 29-39 wt%
Suutala [8]	GTAW	30-300 °C/s	Hammar & Svensson [19]	1.50	35 wt%
Koseki *et al.* [47, 48]	GTAW	N.S.	DeLong modified Cr_{eq} = Cr + 1.5Si + Mo Ni_{eq} = Ni + 30C + 0.5Mn + 18N	1.36 $(1.43)_{H\&S}$	45 wt% $(44\ wt\%)_{H\&S}$
Brooks *et al.* [12, 13]	GTAW	N.S.	Hammar & Svensson [19]	1.51	30 wt%
Anderson *et al.* [28]	GTAW furnace	30 °C/s	Cr_{eq} = Cr + Mo Ni_{eq} = Ni	1.50 $(1.55)_{H\&S}$	37 wt% $(38\ wt\%)_{H\&S}$
Kotecki & Siewert [35]	WRC-1992	N.S.	Cr_{eq} = Cr + Mo + 0.7Nb Ni_{eq} = Ni + 35C + 20N + 0.25Cu	1.42 $(1.55)_{H\&S}$	31 wt% $(30\ wt\%)_{H\&S}$
				1.37 $(1.48)_{H\&S}$	42 wt% $(40\ wt\%)_{H\&S}$
Fe-Cr-Ni phase diagram [46]		Equilibrium conditions	No equivalents. Pure Cr and Ni.	1.67	40 wt%
				1.50	30 wt%
Current research	GTAW furnace	10 °C/s	Hammar & Svensson [19]	1.28-1.32	40 wt%
				1.38-1.55	30 wt%

transitions expected from WRC-1992 diagram [35] and from Fe-Cr-Ni phase diagram have been included in Table 6. The last column in the table shows the alloy level [Cr_{eq}+Ni_{eq}] calculated by the author of the current paper also for comparison purposes. As historically there has not been unanimity in terms of the equivalents used by researchers, here the Hammar and Svensson values have been calculated from compositional data available in previous works and shown in brackets. This enables to have comparative values with the results of the present research.

None of the previous research specifically considered the influence of alloy level [Cr_{eq} + Ni_{eq}] on the [AF]/[FA] transition. Therefore, their investigations either only examined a single alloy or, when different alloys were considered, the total [Cr_{eq} + Ni_{eq}] amount was not taken into consideration. On the contrary, the current research demonstrated that the transition was not only dependant on the Cr_{eq}/Ni_{eq} ratio, but also on the level of alloy [Cr_{eq} + Ni_{eq}]. For every alloy level, the transition is characterised by a range of Cr_{eq}/Ni_{eq} values where both solidification modes coexist, therefore there is not a single critical Cr_{eq}/Ni_{eq} ratio for the transition. It has been demonstrated that at a cooling rate of 10 °C/s, for [Cr_{eq} + Ni_{eq}] = 30 wt%, the transition was found between Cr_{eq}/Ni_{eq} = **1.38 and 1.55** and for [Cr_{eq} + Ni_{eq}] = 40 wt%, the ratios were between Cr_{eq}/Ni_{eq} = **1.28-1.32.** It is concluded that a higher alloy level implies lower Cr_{eq}/Ni_{eq} values and narrower range of coexistence.

From Table 6 it is clear that the critical Cr_{eq}/Ni_{eq} ratio in [AF]/[FA] transition is strongly influenced by the alloy level [Cr_{eq} + Ni_{eq}], as differences in critical ratios found by researchers can be mainly explained by differences in the total level of alloy of the samples studied. Another reason which possibly explains differences between previous results and current ones could be also related to the fact that the cooling rate was not specifically determined nor considered by some researchers. For an alloy level of [Cr_{eq} + Ni_{eq}] = 30 wt%, the critical ratios predicted by WRC-1992, by the Fe-Cr-Ni phase diagram and by Brooks *et al.* fall in the range of values found in the current research, while for [Cr_{eq} + Ni_{eq}] = 40 wt% there are higher discrepancies between the values.

4 Summary

Up to now, the influence of the chemical composition on the austenitic stainless steel solidification modes has been traditionally related to the Cr_{eq}/Ni_{eq} parameter. The experimental results from the current research show that the total level of alloy, i.e. [Cr_{eq} + Ni_{eq}] is also a key parameter to be taken into consideration. It has been found that the higher alloyed series required lower Cr_{eq}/Ni_{eq} values to experience a specific solidification mode. From the results, it is also evident that the higher alloyed series promote the ferritic solidification modes and detriments the

austenitic ones. Regarding the [AF]/[FA] transition, it has been found that for an alloy level of [Cr_{eq}+ Ni_{eq}] = 30 wt%, the critical Cr_{eq}/Ni_{eq} ratio takes place between **1.38 and 1.55.** However, in case of [Cr_{eq}+ Ni_{eq}] = 40 wt%, the critical Cr_{eq}/Ni_{eq} ratio takes place between **1.28 and 1.32.** Therefore, these experimental results show that the transition between [AF]/[FA] solidification modes depends on the alloy level and that the lower alloyed alloys series experiences the transition at higher Cr_{eq}/Ni_{eq} ratios and in a wider interval. It is also clear that there is no abrupt transition or a single Cr_{eq}/Ni_{eq} value where the transition takes place, but a coexistence in a range of samples and values.

Previous research did not consider the effect of the total alloy level [Cr_{eq}+ Ni_{eq}] on the determination of the critical Cr_{eq}/Ni_{eq} ratio, and some of them neither considered the cooling rate conditions, therefore discrepancies in critical ratios between previous research and current one can be explained by this fact.

Acknowledgements

The author gratefully acknowledges the support of Metrode Products Ltd and is especially indebted to Dr. Zhuyao Zhang and Mr. Adam W. Marshall for providing the materials and facilities in order to carry out this research. The current research is part of the Doctoral Degree Thesis entitled "*Modelització del nivell de ferrita δ als acers inoxidables austenítics sotmesos a fusió per arc electric*", which was submitted for the Degree of Doctor in Chemistry by the author at the University of Barcelona the 29th of June 2010. It is also gratefully acknowledged the supervision of Dr. Pere Molera and Dr. Núria Llorca from the Department of Materials Science and Metallurgical Engineering at the University of Barcelona. It is gratefully acknowledged the sponsorship by ESAB for the author's attendance to the IIW 64th Annual Assembly in Chennai and is especially grateful to Dr. Leif Karlsson for his invaluable commitment.

References

[1] Kujanpää V.P., David S.A., White C.L.: Formation of hot cracks in austenitic stainless steel welds- solidification cracking, Welding Journal, 1986, vol. 65, num. 8, p. 203s-212s.

[2] Suutala N., Takalo T. and Moisio T.: The relationship between solidification and microstructure in austenitic and austenitic-ferritic stainless steel welds, Metallurgical Transactions A, 1979, vol. 10A, num. 4, p. 512-514.

[3] Kujanpää V.P., Suutala N., Takalo T. and Moisio T.: Correlation between solidification cracking and microstructure in austenitic and austenitic-ferritic stainless steel welds, Welding Research International, 1979, vol. 9, num. 2, p. 55-75.

[4] Lippold J.C. and Savage W.F.: Solidification of austenitic stainless steel weldments: part III – The effect of solidification behavior on hot cracking susceptibility, Welding Journal, 1982, num. 12, p. 388s-396s.

[5] Brooks J.A., Thomson A.W. and Williams J.C.: Variations in weld ferrite content due to P and S. Welding Journal, 1983, num. 8, p. 220s-225s.

[6] Kujanpää V.P, Suutala N.J., Takalo T.K. and Moisio T.J.I.: Solidification cracking - estimation of the susceptibility of austenitic and austenitic-ferritic stainless steel welds, Metal Construction, 1980, vol. 12, num. 6, p. 282-285.

[7] Suutala N., Takalo T. and Moisio T.: Technical note: Comment on the transformation δ→γ by a massive mechanism in austenitic stainless steel, Welding Journal, 1981, num. 5, p. 92s-93s.

[8] Suutala N.: Effect of solidification conditions on the solidification mode in austenitic stainless steels, Metallurgical Transactions A, 1983, vol 14A, num. 2, p. 191-197.

[9] Kujanpää V.P.: Effects of steel type and impurities in solidification cracking of austenitic stainless steel welds, Metal Construction, 1985, vol. 17, num. 1, p. 40R-46R.

[10] Brooks J.A.: Solidification behavior and cracking susceptibility of austenitic stainless steel welds, Proceedings of the 8th Annual North American Welding Research Conference, Columbus, 19-21 October 1992. Ohio, 1992, 14 pages.

[11] Li L. and Messler R.W.Jr.: The effects of phosphorus and sulphur on susceptibility to weld hot cracking in austenitic stainless steels, Welding Journal, 1999, num. 12, p. 387s-396s.

[12] Brooks J.A., Robino C.V., Headley T.J. and MICHAEL J.R.: Weld solidification and cracking behavior of free-machining stainless steel, Welding Journal, 2003, num. 3, p. 51s-64s.

[13] Brooks J.A., Goods S.H., Robino C.V.: Weld properties of AISI 303 free-machining stainless steel, Welding Journal, 2003, num. 4, p. 84s-92s.

[14] Shankar V., Gill T.P.S., Mannan S.L. and Sundaresan S.: Solidification cracking in austenitic stainless steel welds, Sadhana, 2003, vol. 28, p. 359-382.

[15] Katayama S., Fujimoto T. and Matsunawa A.: Correlation among solidification process, microstructure, microsegregation and solidification cracking susceptibility in stainless steel weld metals, Transactions of Japanese Welding Research Institute, 1985, vol. 14, num. 1, p. 123-138.

[16] Lundin C.D., Delong W.T. and Spond D.F.: Ferrite-fissuring relationship in austenitic stainless steel weld metals. Welding Journal, 1975, num. 8, p. 241s-246s.

[17] Lundin C.D., Delong W.T. and Spond D.F.: The fissure bend test, Welding Journal, 1976, n. 6, p. 145s-151s.

[18] Schaeffler A.L.: Constitution diagram for stainless steel weld metal, Metal Progress, 1949, vol. 56, n. 11, p. 680-680B.

[19] Hammar Ö. and Svensson U.: Influence of steel composition on segregation and microstructure during solidification of austenitic stainless steels. The Metals Society. International Conference on Solidification and Casting of Metals. Sheffield (UK): 1979, p. 401-410.

[20] Long C.J. and Delong W.T.: The ferrite content of austenitic stainless steel weld metal. Welding Journal. 1973, vol. 52, n. 7, p. 281s-297s.

[21] Elmer J.W., Allen S.M. and Eagar T.W.: Microstructural development during solidification of stainless steel alloys. Metallurgical Transactions A. 1989, vol. 20A, p. 2117-2131.

[22] Inoue H., Koseki T. and Ohkita S.: Effect of solidification and subsequent transformation on ferrite morphologies in austenitic stainless steel welds. International Institute of Welding, 1996. Doc. IX-1835. 24 pages. Abstract in English of 5 technical papers published at Quarterly Journal of the Japan Welding Society. 1997, vol. 15, num. 1, p. 77-87, 88-99, num. 2, p. 281-291, 292-304, 305-313.

[23] Inoue H. and Koseki T.: Clarification of solidification behaviors in austenitic stainless steels based on welding process. Nippon Steel Technical Report. 2007, num. 95, p. 62-70.

[24] Inoue H., Koseki T, Ohkita S. and Fuji M.: Formation mechanism of vermicular and lacy ferrite in austenitic stainless steel weld metals. Science and Technology of Welding and Joining. 2000, vol. 5, num. 6, p. 385-396.

[25] Elmer J.W., Allen S.M., Eagar T.W.: The influence of cooling rate on the ferrite content of stainless steel alloys. Proceedings of the 2nd International Conference on Trends in Welding Research, Gatlinburg, 14-18 May 1989. Tennessee: ASM International, 1989, p. 165-170.

[26] Lippold J.C.: Solidification behavior and cracking susceptibility of pulsed-laser welds in austenitic stainless steels. Welding Journal. 1994, num. 6, p. 129s-139s.

[27] Stelling K., Michael T., Schobbert H.: Solidification behaviour and weldability of austenitic steels in laser and hybrid welding. Welding and cutting. 2007, vol. 6, num. 3, p. 171-175.

[28] Anderson T.D., Perricone M.J., DuPont J.N. and MARDER A.R.: The influence of molybdenum on stainless steel weld microstructures. Welding Journal. 2007, vol. 86, num. 9, p. 281s-292s.

[29] Fukumoto S. and Kurz W.: Solidification phase and microstructure selection maps for Fe-Cr-Ni alloys. ISIJ International. 1999, vol. 39, num. 12, p. 1270-1279

[30] Fukumoto S. and Kurz W.: Prediction of the δ to γ transition in austenitic stainless steels during laser treatment. ISIJ International. 1998, vol. 38, num. 1, p. 71-77.

[31] Katayama S. and Matsunawa A.: Solidification microstructure of laser welded stainless steels. Proceedings International Congress on Applications of Lasers & Electro-Optics (ICALEO). Laser Institute of America. 1984, vol. 44, p. 60-67.

[32] Iamboliev T., Katayama S. and Matsunawa A.: Interpretation of phase formation in austentic stainless steel welds. Welding Journal. 2003, num. 12, p. 337s-347s.

[33] Elmer J.W., Eagar T.W. and Allen S.M.: Modeling second-phase formation during rapid resolidification of stainless steel alloys, Conference on Stainless Steels, June 10-13, Chiba. Japan, 1991, 8 p.

[34] Elmer J.W., Eagar T.W. and Allen S.M.: Single-phase solidification during rapid-resolidification of stainless steel alloys. Proceedings of the Materials Weldability Symposium. Ohio: ASM International, 1990, p. 143-150.

[35] Kotecki D.J. and Siewert T.A. WRC-1992: Constitution Diagram for stainless steel weld metals: a modification of the WRC-1988 Diagram, Welding Journal, 1992, num. 5, p. 171s-178s.

[36] Valiente Bermejo M.A.: A mathematical model to predict δ-ferrite content in austenitic stainless steel weld metals, Welding in the World, 2012, vol. 56, issue 09/10, p. 48-68.

[37] ASTM E1306-94 (Reapproved 2004) Standard Practice for Preparation of Metal and Alloy Samples by Electric Arc Remelting for the Determination of Chemical Composition, Philadelphia: ASTM International, 2004.

[38] Valiente Bermejo M.A.: Modelization of δ-ferrite content (FN) in austenitic stainless steels under electric arc conditions, PhD, University of Barcelona. Department of Materials Science and Metallurgical Engineering, June 2010. ISBN 978-84-693-5713-2.

[39] ASTM E1306-07 Standard Practice for Preparation of Metal and Alloy Samples by Electric Arc Remelting for the Determination of Chemical Composition. Philadelphia: ASTM International, 2007.

[40] Lippold J.C. and Kotecki D.J.: Welding Metallurgy and Weldability of Stainless Steels, New Jersey: Wiley-Interscience, 2005. ISBN 0-471-47379-0.

[41] Rajasekhar K., Harendranath C.S., RAMAN R. and Kulkarni S.D.: Microstructural evolution during solidification of austenitic stainless steel weld metals: a color

metallographic and electron microprobe analysis study, Materials Characterization, 1997, vol. 38, num. 2, p. 53-65.

[42] Tosten M.H. and Morgan M.J.: Microstructural study of fusion welds in 304L and 21Cr-6Ni-9Mn stainless steels, Westinghouse Savannah River Company, 2005, ref. TR-2004-00456, 27 pages.

[43] Smith J.J. and Farrar R.A.: Influence of microstructure and composition on mechanical properties of some AISI 300 series weld metals, International Materials Reviews, 1993, vol. 38, num. 1, p. 25-50.

[44] Oseki T., Matsumiya T., Yamada W. and Ogawa T.: Numerical modeling of solidification and subsequent transformation of Fe-Cr-Ni alloys, Metallurgical and Materials Transactions A, 1994, vol. 25A, p. 1309-1321.

[45] Kundrat D.M. and Elliot J.F.: Phase relationships in the Fe-Cr-Ni system at solidification temperatures, Metallurgical Transactions A., 1988, vol. 19A, p. 899-908.

[46] Folkhard E.: Welding Metallurgy of Stainless Steels. Vienna: Springer-Verlag, 1988. ISBN 3-211-82043-4.

[47] Ogawa T. and Koseki T.: Weldability of newly developed austenitic alloys for cryogenic service: Part II- High-nitrogen stainless steel weld metal, Welding Journal, 1988, vol. 67, num. 1, p. 8s-17s.

[48] Koseki T., Inoue H., Morimoto H. and Ohkita S.: Prediction of solidification and phase transformation of stainless steel weld metals, Nippon Steel Technical Report, 1995, num. 65, p. 33-40.